iScience, Volume *26*

Supplemental information

Stability of high-entropy alloys under electrocatalytic conditions

Attila Kormányos, Qi Dong, Bin Xiao, Tangyuan Li, Alan Savan, Ken Jenewein, Tatiana Priamushko, Andreas Körner, Thomas Böhm, Andreas Hutzler, Liangbing Hu, Alfred Ludwig, and Serhiy Cherevko

Thin film	Pt_{RF} (W)	Ru_{DC} (W)	Ir_{DC} (W)	Rh_{RF} (W)	Pd_{RF} (W)
Pt					
PtRu	170	75			
PtRuIr	167	66	57		
PtRuIrRh	173	58	50	168	
PtRuIrRhPd	190	69	59	193	156

Table S1. Sputter parameters for unary Pt, binary PtRu, ternary PtRuIr, quaternary PtRuIrRh and quinary PtRuIrRhPd thin films, respectively. Related to Figure 1.

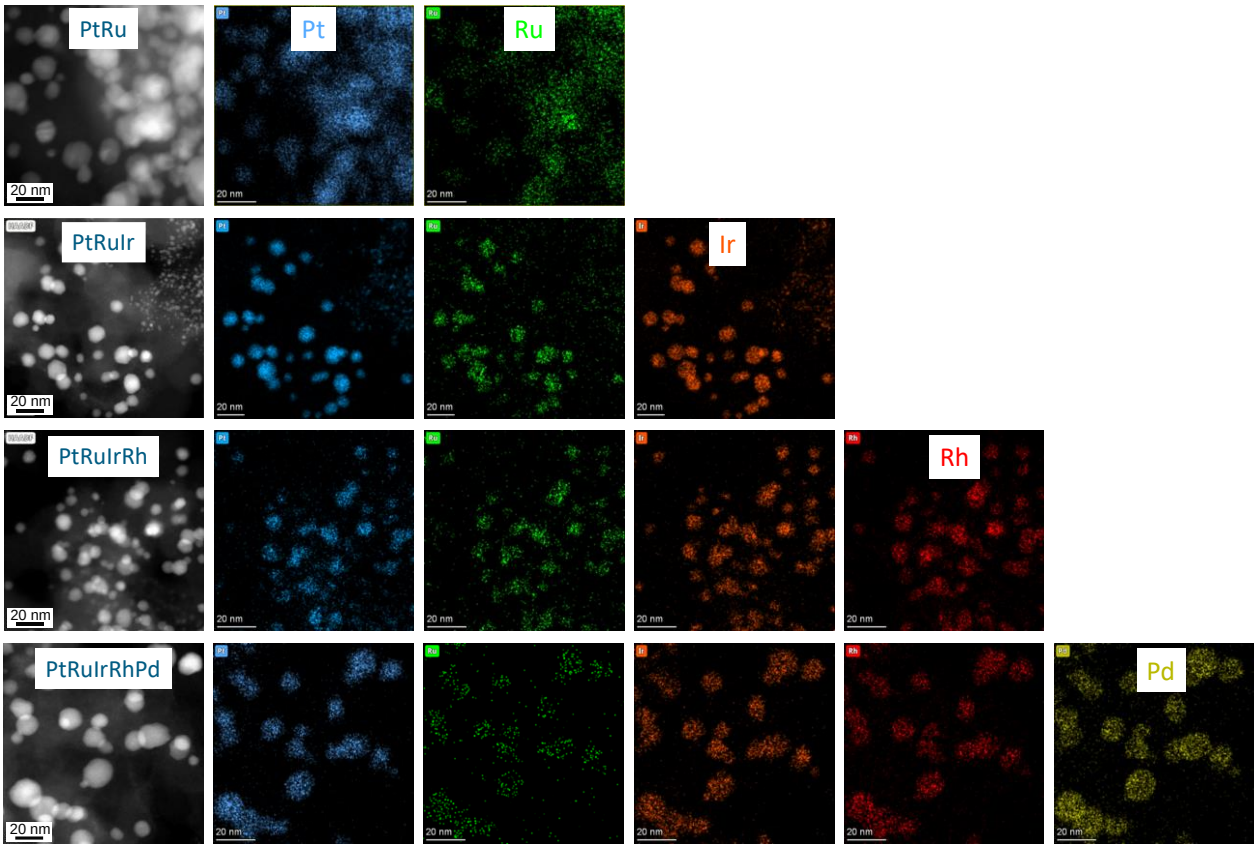

Figure S1.: HAADF-STEM and EDX spectrum imaging results gathered for all multimetallic carbon-supported samples. Related to Figure 1.

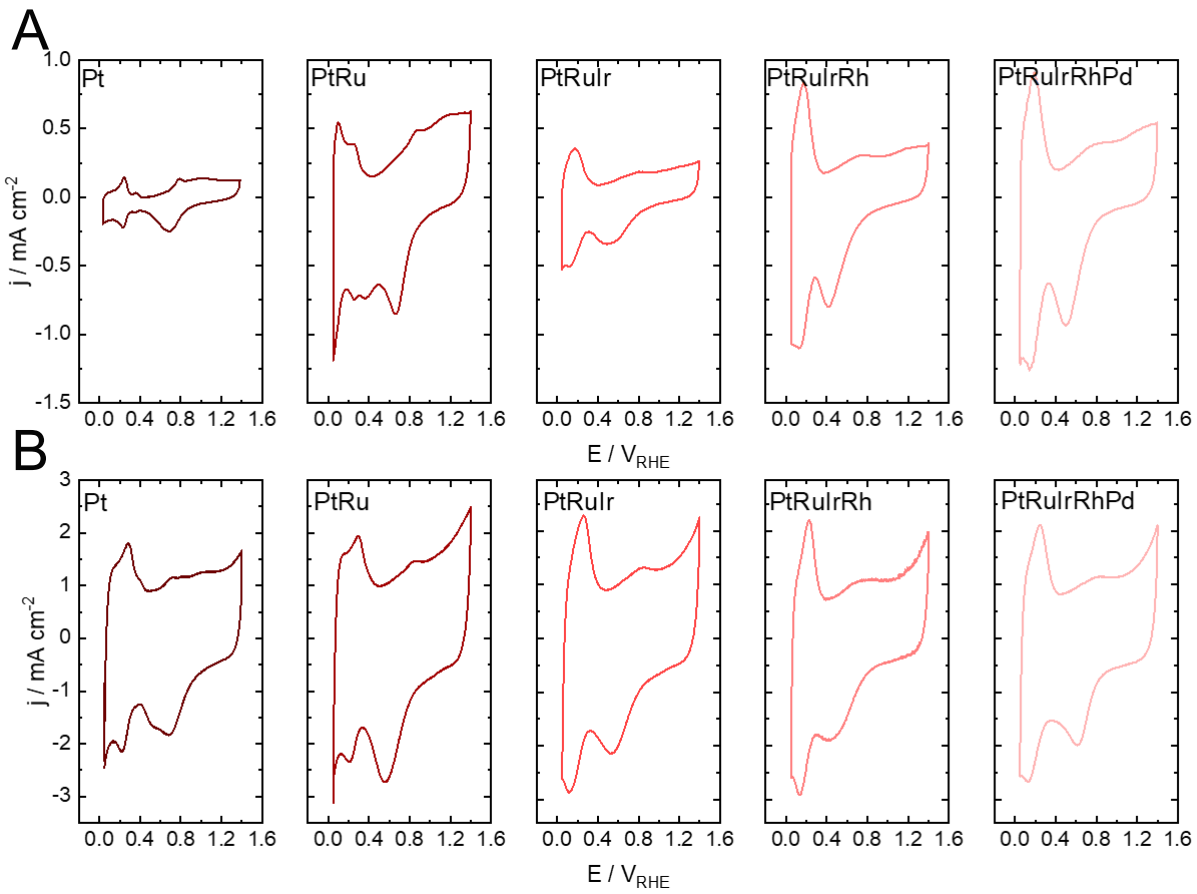

Figure S2. Cyclic voltammetry results recorded for all samples ranging from unary to quinary compositions. (A) CVs recorded for the sputtered thin films and (B) for the carbon-supported nanoparticles in 0.05 M KOH electrolyte solution in between 0.05 V_{RHE} and 1.4 V_{RHE}, applying 200 mV s^{-1} scan rate. The electrolyte solution was saturated with Ar. Related to Figure 2.

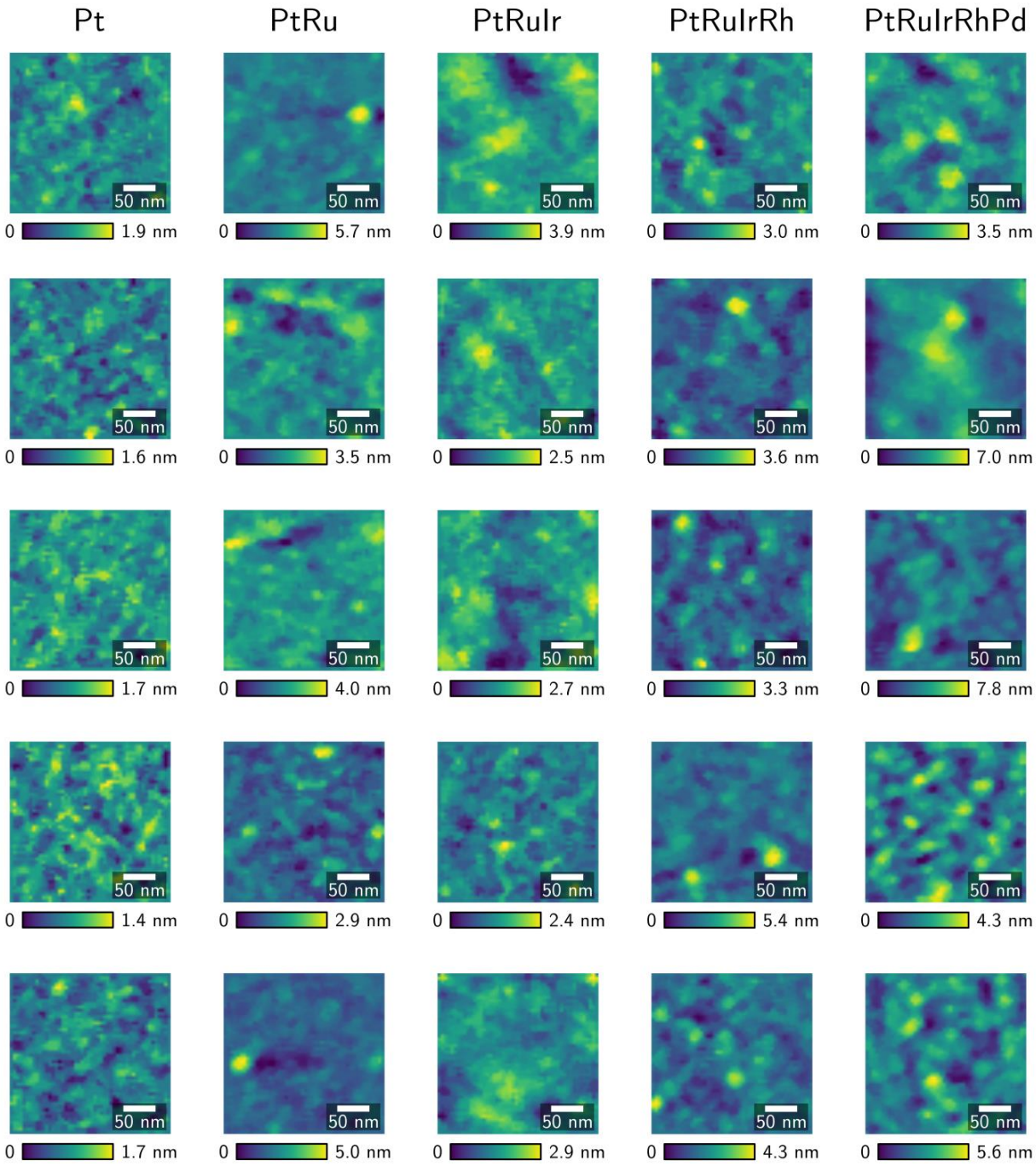

Fig. S3. AFM topography images of the samples. AFM imaging in contact mode was performed on five spots per sample. An image area of 0.25 x 0.25 µm² was recorded at a pixel size of 5 nm per spot. The images represent the topography of the samples, with the intensity distribution equaling the full sample height distribution. The raw data were corrected for sample tilt by a line slope subtraction, and the images were processed by a 3 x 3 median filter to remove single-pixel outliers. Related to Figure 2.

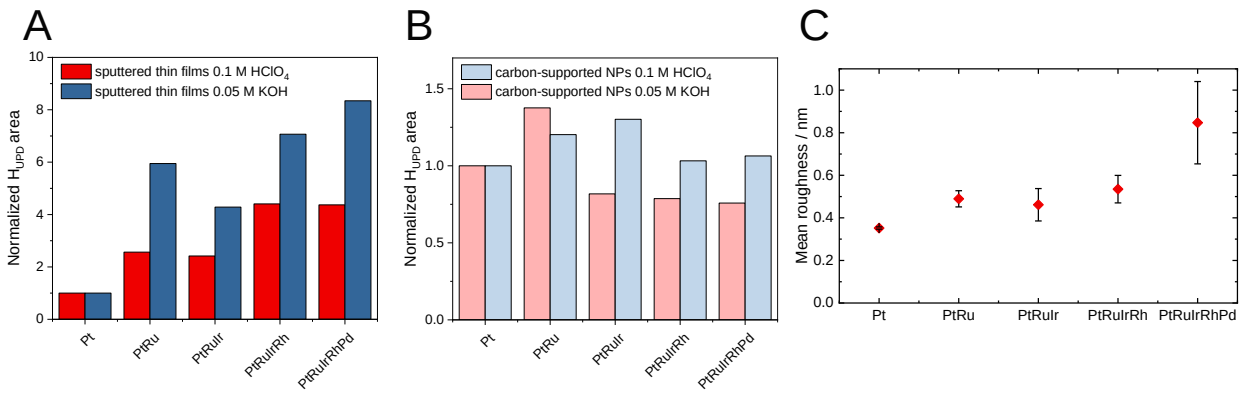

Fig. S4. Normalized H_{UPD} area and mean roughness calculated form the cyclic voltammograms and AFM measurements. (A) H_{UPD} area that was determined for the sputtered thin films and (B) for the carbon-supported nanoparticles in 0.1 M $HClO_4$ and 0.05 M KOH electrolyte solution from the cyclic voltammograms presented in Figure 2 and S1. (C) Mean surface roughness (Ra) from thin films. Arithmetic mean values ± standard deviation from five scans per sample are displayed. Related to Figure 2.

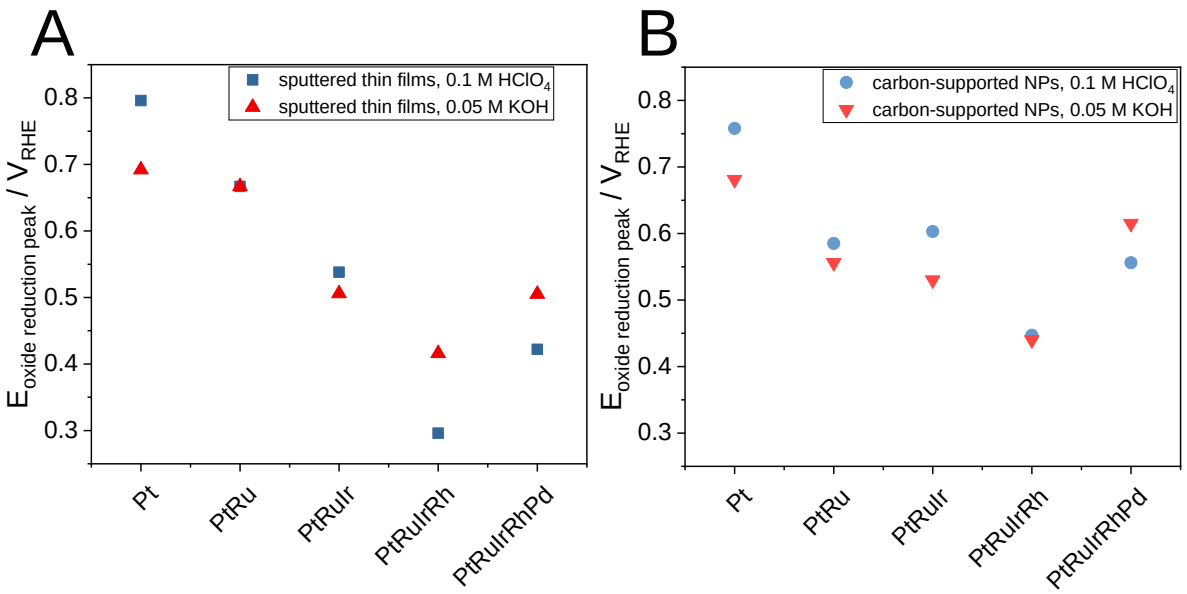

Fig. S5. Half wave potential of the oxide reduction peaks derived from the cyclic voltammograms. (A) Oxide reduction peak potentials were determined for the sputtered thin films and (B) for the carbon-supported nanoparticles in 0.1 M $HClO_4$ and 0.05 M KOH electrolyte solution. The electrolyte solutions were saturated with Ar. Related to Figure 2.

Stability of pristine metals in acidic and alkaline media

O*n-line* ICP-MS results are presented for each pristine metal. Identical electrochemical protocols as for the alloys were performed. All presented data were recorded for thin-film samples. Each figure is followed by a short discussion of the observed dissolution feature(s). The onset potential of anodic dissolution is also presented in each figure showing results for the protocol (A).

Platinum:

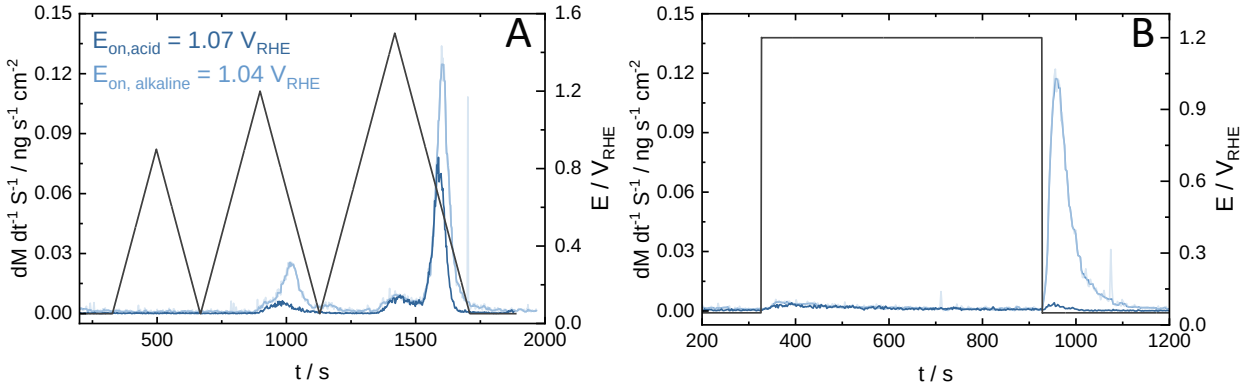

Fig. S6. Stability of Pt thin films. The stability of Pt was mapped in Ar-saturated acidic (dark blue curves) and in alkaline (pale blue curves) electrolytes under two electrochemical protocols: (A) three CVs starting at 0.05 V_{RHE} with gradually increasing upper potential limits (UPL) of 0.9-, 1.2-, 1.5 V_{RHE} applying 5 mV s^{-1} scan rate. (B) 5 min hold at 0.05 V_{RHE} followed by a 10 min hold at 1.2 V_{RHE}. The protocol is finished with a 5 min hold at 0.05 V_{RHE}. Related to Figure 3-5.

Protocol (A)
Dissolution of Pt was observed only if the UPL exceeded 0.9 V_{RHE}.
Two dissolution features are visible: [1-3]

1. Transient dissolution during the forward scan (“anodic dissolution”) – formation of a PtO_x surface layer, place exchange, and surface passivation.
2. Transient dissolution during the reverse scan (“cathodic dissolution”) – reduction of the previously formed PtO_x layer.

The measured dissolution rates are notably smaller in the case of anodic dissolution compared to the values measured during the reverse scan.

Difference between acidic and alkaline electrolytes: anodic dissolution rates are similar, while notably higher cathodic dissolution was detected when measurements were performed in 0.05 M KOH. This change in dissolution rates possible emerged due to the variation in the life-times of the formed intermediates, the change in solubility of these intermediates and due to the difference in the amount of the formed PtO_x.[1]

Protocol (B)
Similar to the CVs, two dissolution features were observed. However, cathodic dissolution for the 0.05 M KOH case is significantly higher compared to the acidic electrolyte. The reason behind the difference is probably due to the applied electrochemical protocol: instead of sweeping slowly back the potential to the starting value a fast potential step was applied. As we showed previously, if the potential step was replaced with a slow sweep to the same potential (kinetics of oxide reduction is controlled), difference between cathodic dissolution tracked in acidic and alkaline media vanishes. This means that the reduction of the formed PtO_x is more sluggish in alkaline conditions, leading to the undercoordinated Pt sites staying longer on the surface of Pt resulting in higher measured dissolution.[4]

Ruthenium:

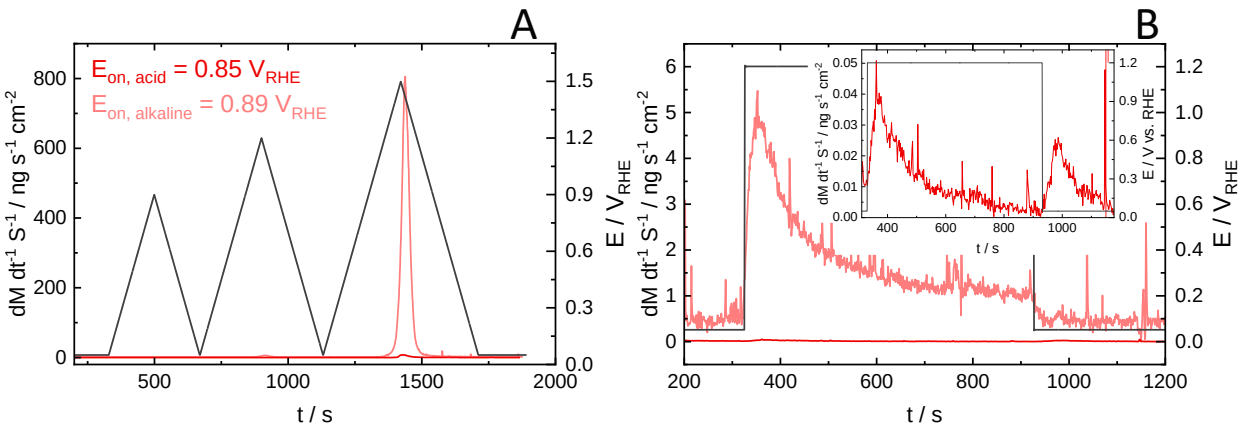

Fig. S7. Stability of Ru thin films. Stability of Ru was mapped in Ar-saturated acidic (dark red curves) and in alkaline (pale red curves) electrolytes under two electrochemical protocols: (A) three CVs starting at 0.05 V_{RHE} with gradually increasing upper potential limits of 0.9-, 1.2-, 1.5 V_{RHE} applying 5 mV s^{-1} scan rate. ^{98}Ru (the least abundant Ru isotope) was tracked in the case of this protocol in alkaline medium. Measurement of ^{102}Ru was not possible due to reaching the detector limit of the ICP-MS. (B) 5 min hold at 0.05 V_{RHE} followed by a 10 min hold at 1.2 V_{RHE}. The protocol is finished with a 5 min hold at 0.05 V_{RHE}. Related to Figure 3-5.

Protocol (A)

Note: Ru dissolution was so severe in alkaline media that there instead of ^{102}Ru (31.6% abundance), another isotope, ^{98}Ru was tracked (1.88% abundance). Very small Ru dissolution was already detected during the reverse scan when the UPL was 0.9 V_{RHE}, which originated from the reduction of various Ru oxide species (probably $RuO_2 \cdot H_2O$, $Ru(OH)_3$).

Two dissolution features are visible:[5,6]
If UPL is not higher than 1.2 V_{RHE}

1. Small anodic dissolution starting at slightly higher potentials compared to thermodynamics (0.74 V_{RHE} in 0.1 M $HClO_4$).[7] Formation of various Ru oxides ($RuO_2 \cdot H_2O$, $Ru(OH)_3$), place-exchange, very fast surface passivation.
2. Cathodic dissolution corresponding to the reduction of the previously formed RuO_x species.

Higher UPLs:

3. If UPL = 1.5 V_{RHE} – only one dissolution peak: instead of transient anodic dissolution constant dissolution of Ru can be observed. This is due to the formation of RuO_4^{2-} species, which is thermodynamically unstable causing constant Ru dissolution (chemical/direct anodic dissolution).[5,7]

Similar to Pt, dissolution of Ru is much higher in alkaline electrolytes compared to the acidic one. This is especially visible when the UPL was 1.5 V_{RHE}. Here, Ru constantly dissolved, almost hitting the detector limit even when its isotope with the lowest abundance was measured.

Protocol (B)

Dissolution in alkaline electrolytes is much higher than at acidic pH. However, here the applied potential was only moderately high (1.2 V_{RHE}) Additionally, a very small cathodic dissolution peak can be seen both in acidic-, and alkaline media underlining that Ru oxides are extremely stable toward reduction.[2] Quantification of these small dissolution features after this rapid reduction step is rather difficult since the observed dissolution can originate from the tailing of the anodic dissolution and cathodic dissolution.[4]

Iridium:

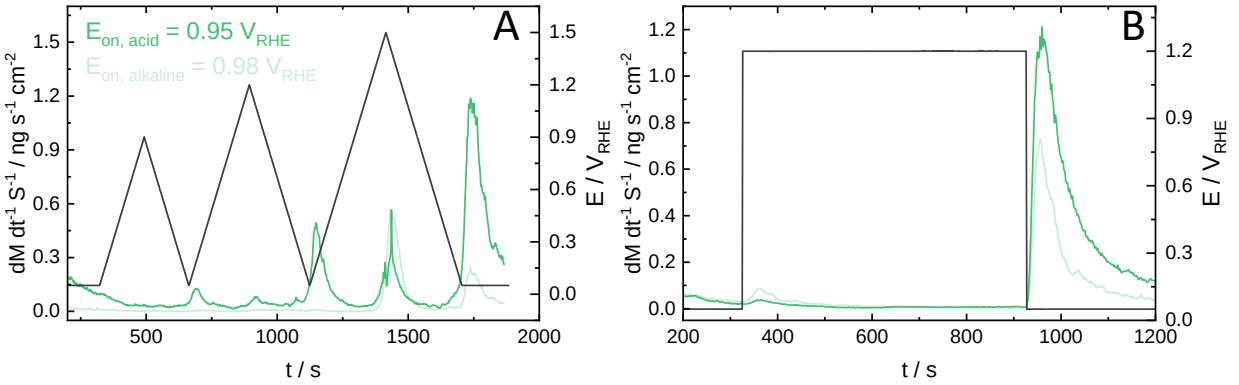

Fig. S8. Stability of Ir thin films. Stability of Ir was mapped in Ar-saturated acidic (dark green curves) and in alkaline (pale green curves) electrolytes under two electrochemical protocols: (A) three CVs starting at 0.05 V_{RHE} with gradually increasing upper potential limits of 0.9-, 1.2-, 1.5 V_{RHE} applying 5 mV s^{-1} scan rate. (B) 5 min hold at 0.05 V_{RHE} followed by a 10 min hold at 1.2 V_{RHE}. The protocol is finished with a 5 min hold at 0.05 V_{RHE}. Related to Figure 3-5.

Protocol(A)
Ir dissolution can be already observed on the reverse scan of the first CV (when the UPL was set to 0.9 V_{RHE}). This corresponds to the reduction of a native Ir oxide layer, which did not get dissolved during the contacting procedure.[8]

Dissolution features:

1. Anodic dissolution corresponding to the oxidation of Ir and the formation of IrO_2. The determined onset potential values match well with the ones reported previously[9,10] and they also correlate with the ones expected from thermodynamics[7] for the formation of the Ir^{3+}/Ir^0 redox couple.
2. Cathodic dissolution peak corresponding to the reduction of the various Ir surface oxides

The difference in stability in acidic and alkaline electrolytes is less pronounced except when the *UPL* = 1.5 V_{RHE}. While in 0.1 M $HClO_4$ anodic dissolution is smaller than the cathodic one, this trend reverses when the electrolyte is switched to 0.05 M KOH.
For further information on Ir dissolution see refs. [10,11]

Protocol (B)
Anodic dissolution is rather small both in acidic and alkaline media thanks to the strong Ir-Ir bond strength (the cohesive energy of Ir atoms is the highest among the metals investigated in our manuscript).[4] This results in the rapid formation of a very thin IrO_2 layer and fast surface passivation. Thus, dissolution rapidly decreases during the hold at 1.2 V_{RHE}. The observed high dissolution rates during the reductive step (at 0.05 V_{RHE}) can be explained in a similar manner as for Pt.

Rhodium:

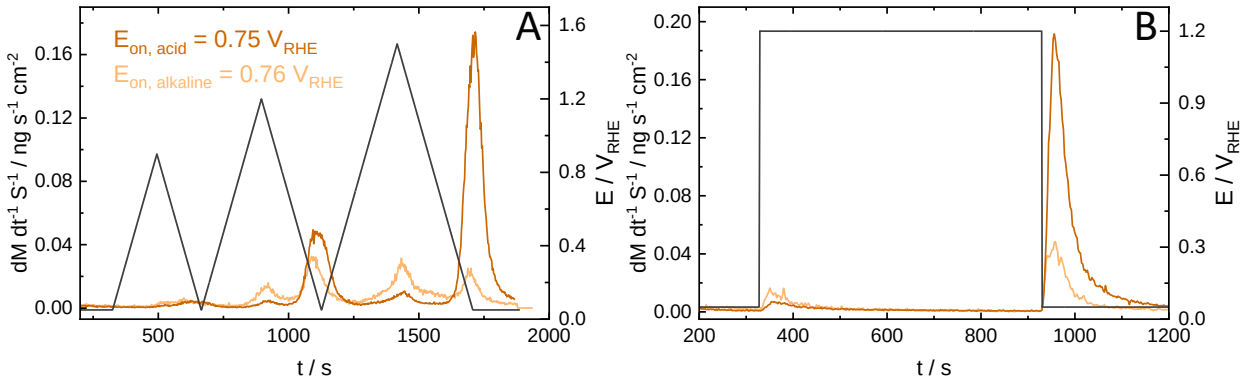

Fig. S9. Stability of Rh thin films. Stability of Rh was mapped in Ar-saturated acidic (dark brown curves) and in alkaline (light brown curves) electrolytes under two electrochemical protocols: (A) three CVs starting at 0.05 V_{RHE} with gradually increasing upper potential limits of 0.9-, 1.2-, 1.5 V_{RHE} applying 5 mV s^{-1} scan rate. (B) 5 min hold at 0.05 V_{RHE} followed by a 10 min hold at 1.2 V_{RHE}. The protocol is finished with a 5 min hold at 0.05 V_{RHE}. Related to Figure 3-5.

Since Rh is the least abundant metal among the ones studied in our manuscript in combination with the fact that it is not applied widely in the field of electrocatalysis, much less information can be found on its stability in the literature.

Protocol (A)
Dissolution rates are similar to Pt. Two main dissolution peaks were observed:

1. Oxide formation – various solid-solid transformations possibly based on the Pourbaix diagram of Rh[7]. The resulting oxides can be: Rh_2O, RhO, Rh_2O_3. The onset potential of dissolution is slightly lower than what was previously measured for polycrystalline Rh in 0.05 M NaOH (0.87 V_{RHE}).[5] No such data is available in acidic electrolytes.
2. Reduction of the formed oxide layer accompanied by cathodic dissolution.

Anodic dissolution is manifested as a small, wide signal, which is followed by a notably higher cathodic dissolution. While the ratio between the cathodic and anodic dissolution is relatively big (especially when *UPL* = 1.5 V_{RHE}) in 0.1 M $HClO_4$ electrolyte, there is much less difference in the magnitude of anodic and cathodic dissolution in alkaline electrolyte. A similar relationship was found for polycrystalline Rh foil in 0.05 M NaOH electrolyte solution.[4]

Protocol (B)
Anodic dissolution is low both in acidic and alkaline media, similar to what one can observe for Pt and Ir and it can be explained on a similar basis (high M-M bond strength). Contrastingly, notable cathodic dissolution can be seen, especially in acidic media. Based on thermodynamics (M-O bond strength $\Delta H_{O,ads}$ = 0.44 eV)[12] the reduction of the formed oxide layer should be fast. Hence, low cathodic dissolution should be detected. More investigations would be needed to fully understand factors governing Rh stability.

Palladium:

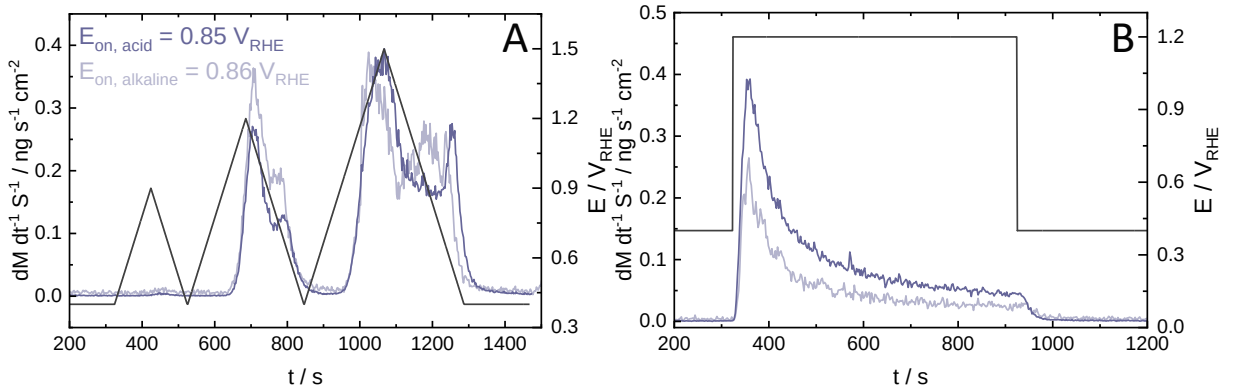

Fig. S10. Stability of Pd thin films. Stability of Pd was mapped in Ar-saturated acidic (dark purple curves) and in alkaline (pale purple curves) electrolytes under two electrochemical protocols: (A) three CVs starting at 0.4 V_{RHE} with gradually increasing upper potential limits of 0.9-, 1.2-, 1.5 V_{RHE} applying 5 mV s^{-1} scan rate. (B) 5 min hold at 0.4 V_{RHE} followed by a 10 min hold at 1.2 V_{RHE}. The protocol is finished with a 5 min hold at 0.4 V_{RHE}. Related to Figure 3-5.

Note: To avoid Pd hydride formation, the starting potential was replaced from 0.05 V_{RHE} to 0.4 V_{RHE} for the pristine Pd samples in all applied protocols.[13,14] This was not an issue for Pd as a constituent of the HEA sample. Thus, electrochemical protocols were kept similar for all alloy samples.

Protocol (A)
Small amount of Pd dissolution can be already detected for *UPL* = 0.9 V_{RHE}. The determined onset potentials both in 0.1 M $HClO_4$ and in 0.05 M KOH are in good agreement with the ones reported previously. [5,15]
Dissolution peaks:

1. Formation of PdO, anodic dissolution. If the UPL is higher than 1.28 V_{RHE}, the formation of PdO2 is also possible (manifested as a shoulder on the anodic peak in the cited literature). Here, the anodic dissolution peaks are notably widened for *UPL* = 1.5 V_{RHE}. Separation of the two dissolution processes is possible if lower scan rate is used.

Acidic medium

2. Only one cathodic dissolution peak can be seen at all applied UPLs. This is in contrast with previous reports.[15] However, the applied scan rate in our case was considerably higher, which might have caused the appearance of a single peak. This peak corresponds to the reduction of PdO_2 and PdO to Pd.

Alkaline medium[5]

2a. Cathodic dissolution. Reduction of surface PdO_2 to PdO in parallel with Pd dissolution.
2b. Cathodic dissolution. Reduction of the remaining PdO to Pd accompanied with Pd dissolution.

Stability of Pd is more or less similar in acidic and alkaline media both qualitatively (dissolution profiles) and quantitatively (magnitude of dissolution rates).

Protocol (B)
The observed dissolution profile and the trends in acidic and alkaline media match well with previous literature data on polycrystalline Pd foil.[4]

The relatively high anodic dissolution can be explained by the moderate strength of the Pd-Pd bonds (E_{coh} = 3.70 eV).[12] Since Pd binds O atoms as strongly as Pt ($\Delta H_{O,ads}$ = 1.53 eV),[12] its surface gradually gets passivated over time causing the decrease of the dissolution rate. Finally, we turn our attention to cathodic dissolution, which is significantly smaller for Pd than the anodic dissolution. Following our previous reasoning, one would expect extensive Pd dissolution when the potential was switched back to 0.4 V_{RHE}, due to its high $\Delta H_{O,ads}$ value. Similar to Rh, additional research efforts would be needed to clarify this discrepancy.

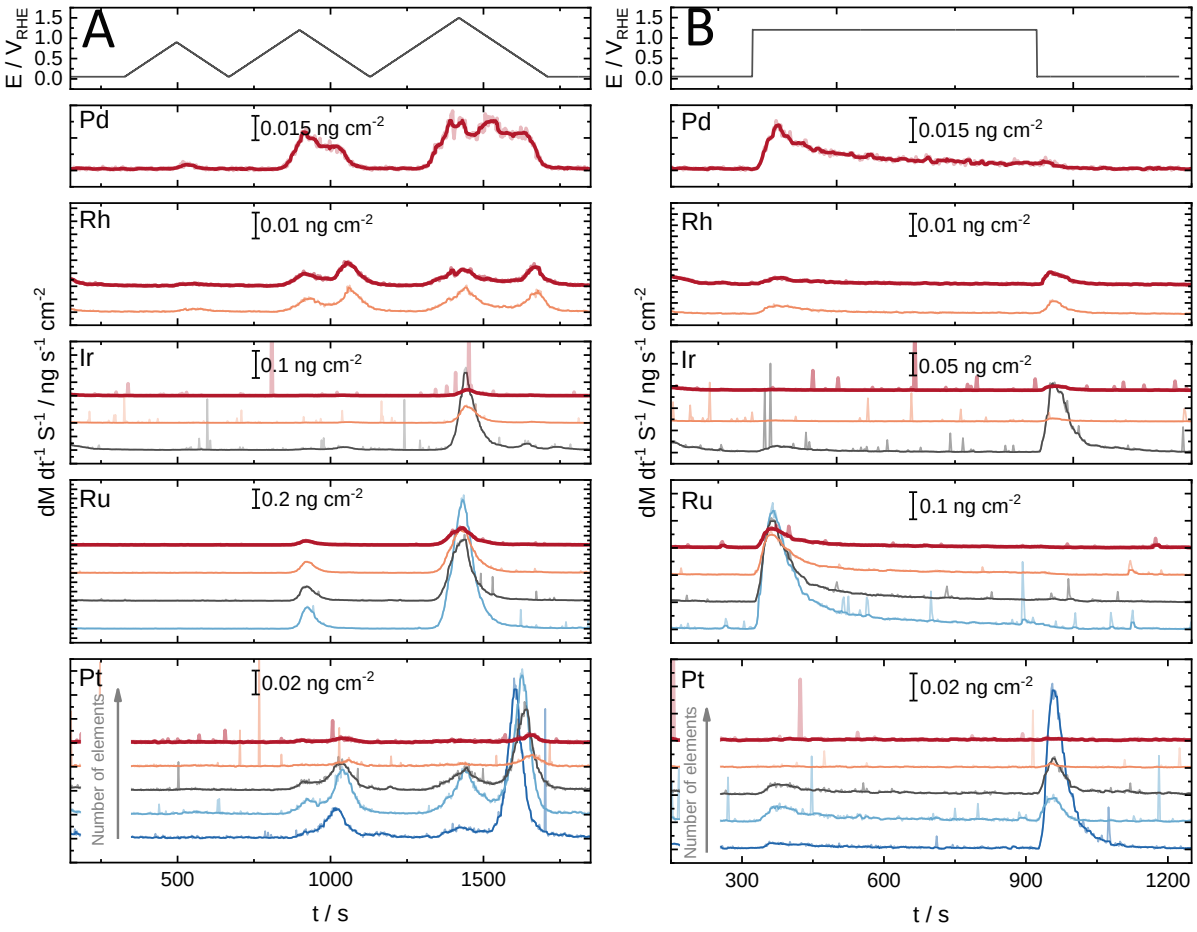

Fig. S11. Dissolution profiles recorded for the *thin film samples* in alkaline electrolyte. (A) The protocol consisted of a 5 min hold at 0.05 V_{RHE}, which was followed by three consecutive CVs with gradually increasing upper potential limits (0.9, 1.2 and 1.5 V_{RHE}) applying 5 mV s^{-1} scan rate. The protocol was finished with a three min potentiostatic hold at 0.05 V_{RHE}. (B) The protocol started with a five min hold at 0.05 V_{RHE}, which was followed by an additional potentiostatic hold for ten minutes at 1.2 V_{RHE}. The measurement was finished with a five min potentiostatic hold at 0.05 V_{RHE}. The electrolyte was 0.05 M KOH in the case of both protocols and it was saturated with Ar during the measurements. In each panel, the dissolution profile at the bottom corresponds to either the pristine metal (only for Pt) or to the alloy comprised of the lowest number of elements. The topmost dissolution profile for each element corresponds to the PtRuIrRhPd HEA sample (red, in bold). Dissolution curves were smoothed as needed using an FFT filter (points of window = 5-8). The original dataset is presented behind the smoothed profile with 50% transparency. Related to Figure 3.

Figure S12 shows the dissolved amounts determined for the CVs in acidic (left two columns) and in alkaline (two columns on the right) media. The amount of the dissolved metals shows a decrease with the increase of alloy constituents (decrease in the molar fraction of the given metal in the alloy) when measurements were conducted in 0.1 M $HClO_4$. The only exception is Rh, where dissolution remained similar for the pure metal and for the quaternary (PtRuIrRh) and quinary (PtRuIrRhPd) alloy. NDA yield a different trend. In the case of Pt, the NDA first increased, which was followed by a decrease to reach similar values to the pure Pt sample. When the UPL was 1.2 V_{RHE}, NDA determined for Ru remained identical. If the potential was increased to 1.5 V_{RHE} a notable decrease in NDA was observed for the PtRu sample (approx. one magnitude), after which slightly smaller values were calculated. Normalized Ir dissolution for the quaternary and quinary alloy is clearly smaller than the ones resulted for the ternary alloy and the pure Ir sample. Rh is the only metal where alloying caused a notable increase in NDA (thanks to the identical dissolved amounts measured for the pure and alloy samples). If the UPL was kept 1.2 V_{RHE}, normalized Pd dissolution for the quinary alloy was a bit smaller, while if the UPL was increased to 1.5 V_{RHE}, it showed similar values to pristine Pd.

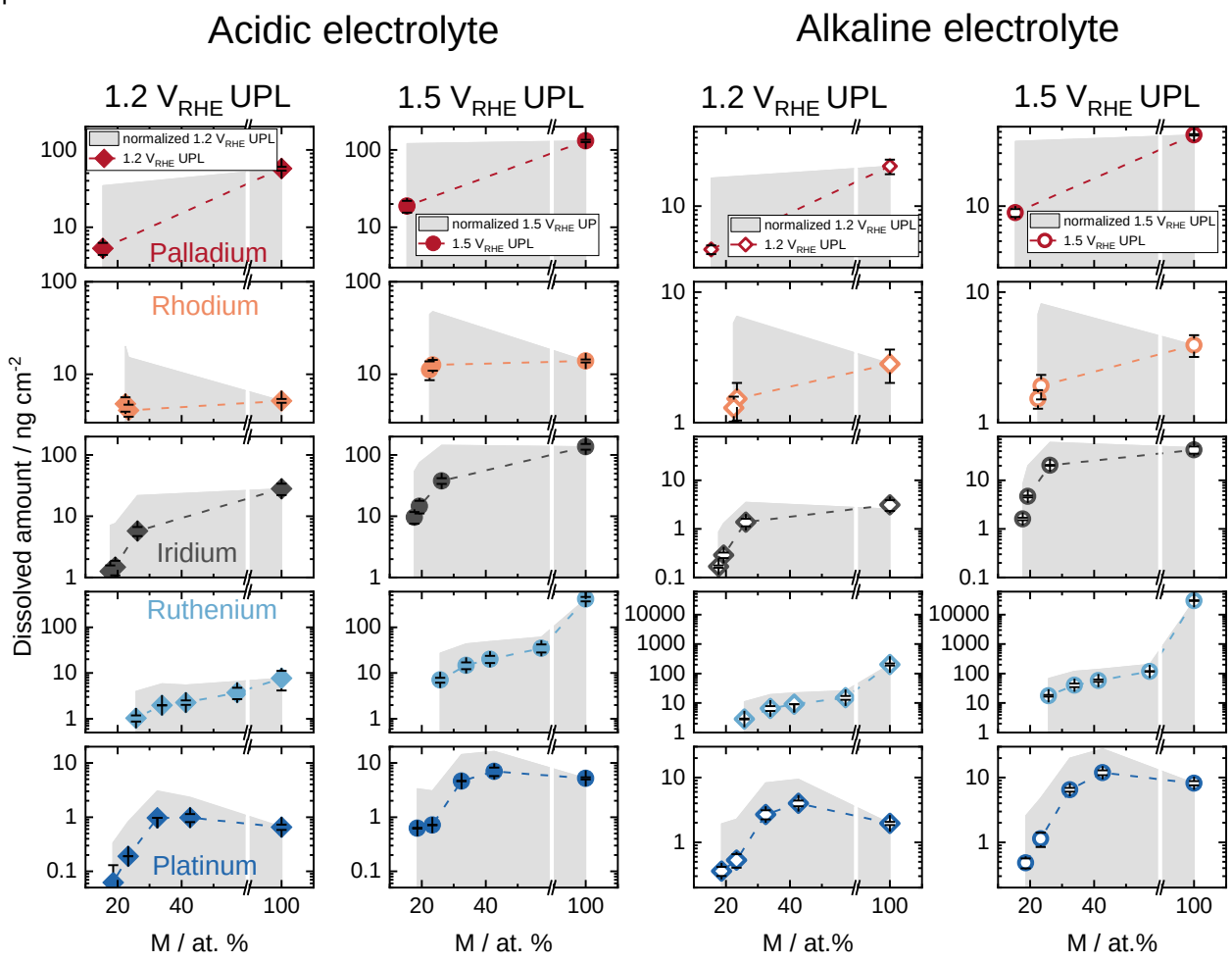

Fig. S12. Dissolved amounts for each alloy constituent as the function of the molar fraction of the given element in the *sputtered thin-film* samples. Left two columns: dissolved amounts as the function of the molar fraction of the given element in the alloy samples. Dissolved amounts were calculated by integrating the dissolution profiles presented in Figure 3A (0.1 M $HClO_4$ electrolyte). Two columns on the right: dissolved amounts as the function of the molar fraction of the given element in the alloy samples. Dissolved amounts were calculated by integrating the dissolution profiles presented in Figure S11A (0.05 M KOH electrolyte Full and hollow diamonds – dissolved amount of the given metal during the second cycle *UPL* = 1.2 V_{RHE}, full and hollow circles – dissolved amount of the given metal during the second cycle *UPL* = 1.5 V_{RHE}, Dashed lines connecting the data points are only serving as a guide for the eye. The grey shaded

area represents the normalized dissolved amounts determined by dividing the calculated dissolved amounts with the molar fraction of the given element in the given alloy. Nominal alloy composition was determined by XPS measurements. Error bars were calculated from at least two separate measurements; each was performed on a fresh catalyst spot. Related to Figure 4.

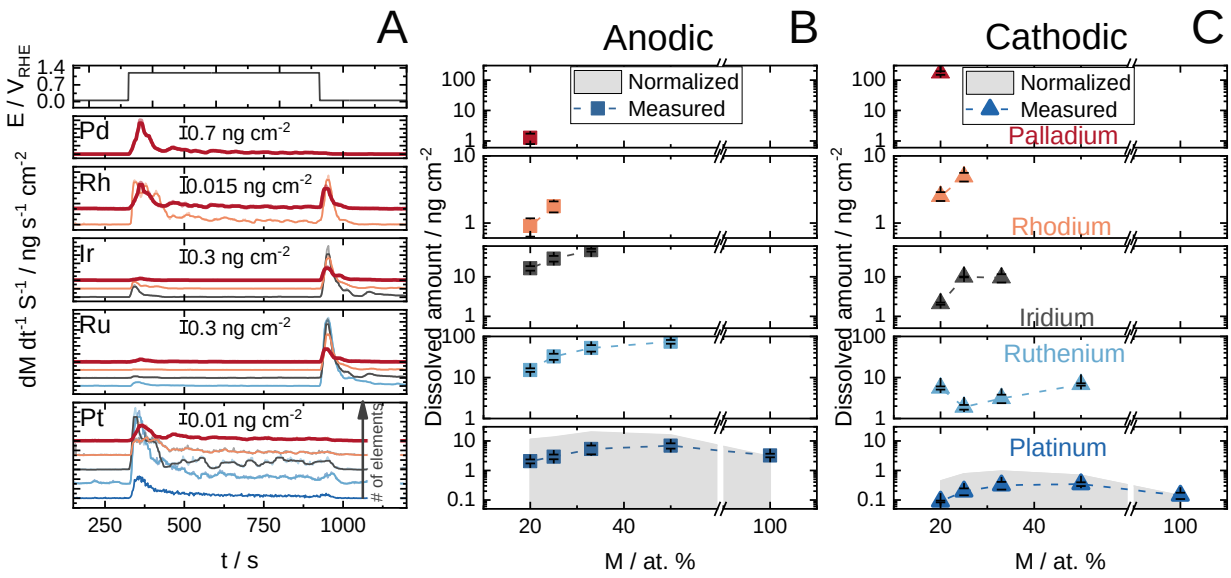

Fig. S13. Dissolution profiles recorded for the *carbon-supported metal alloy nanoparticles* in acidic media and the calculated dissolved amounts as the function of the molar fraction of each metal in the alloy samples. (A) The protocol started with a five min hold at 0.05 V_{RHE}, which was followed by an additional potentiostatic hold for ten minutes at 1.2 V_{RHE}. The measurement was finished with a five min potentiostatic hold at 0.05 V_{RHE}. The electrolyte was 0.1 M $HClO_4$ in the case of both protocols and it was saturated with Ar during the measurements. In each panel, the dissolution profile at the bottom corresponds to either the pristine metal (only for Pt) or to the alloy comprised of the lowest number of elements. The topmost dissolution profile for each element corresponds to the PtRuIrRhPd HEA sample (red, in bold). Dissolution profiles were smoothed using an FFT filter (points of window = 5-8). The original dataset is presented behind the smoothed profile with 50% transparency. (B) and (C) Dissolved amounts as the function of the molar fraction of the given element in the alloy samples. Dissolved amounts were calculated by integrating the dissolution profiles presented in Figure S13A (0.1 M $HClO_4$ electrolyte). Squares – dissolved amount of the given metal during the potentiostatic hold at 1.2 V_{RHE}, Triangles – dissolved amount of the given metal during the potentiostatic hold at 0.05 V_{RHE}. The grey shaded area represents the normalized dissolved amounts determined by dividing the calculated dissolved amounts with the molar fraction of the given element in the given alloy. Error bars were calculated from at least two separate measurements; each was performed on a fresh catalyst spot. Related to Figure 5.

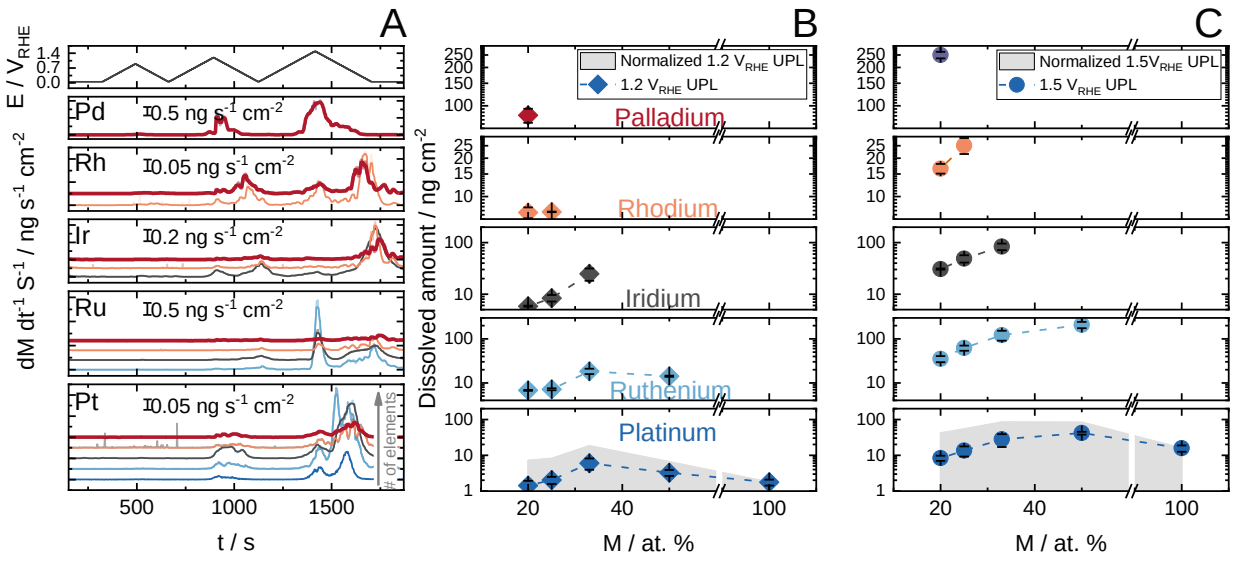

Fig. S14. Dissolution profiles recorded for the *carbon-supported metal alloy nanoparticles* in acidic media and the calculated dissolved amounts as the function of the molar fraction of each metal in the alloy samples. (A) The protocol started with a five min hold at 0.05 V_{RHE}, which was followed by an additional potentiostatic hold for ten minutes at 1.2 V_{RHE}. The measurement was finished with a five min potentiostatic hold at 0.05 V_{RHE}. The electrolyte was 0.1 M $HClO_4$ in the case of both protocols and it was saturated with Ar during the measurements. In each panel, the dissolution profile at the bottom corresponds to either the pristine metal (only for Pt) or to the alloy comprised of the lowest number of elements. The topmost dissolution profile for each element corresponds to the PtRuIrRhPd HEA sample (red, in bold). Dissolution profiles were smoothed using an FFT filter (points of window = 5-8). The original dataset is presented behind the smoothed profile with 50% transparency. (B) and (C) Dissolved amounts as the function of the molar fraction of the given element in the alloy samples. Dissolved amounts were calculated by integrating the dissolution profiles presented in Figure 14A (0.1 M $HClO_4$ electrolyte). Full diamonds – dissolved amount of the given metal during the second cycle *UPL* = 1.2 V_{RHE}, full circles – dissolved amount of the given metal during the second cycle *UPL* = 1.5 V_{RHE}. The grey shaded area represents the normalized dissolved amounts determined by dividing the calculated dissolved amounts with the molar fraction of the given element in the given alloy. Error bars were calculated from at least two separate measurements; each was performed on a fresh catalyst spot. Related to Figure 5.

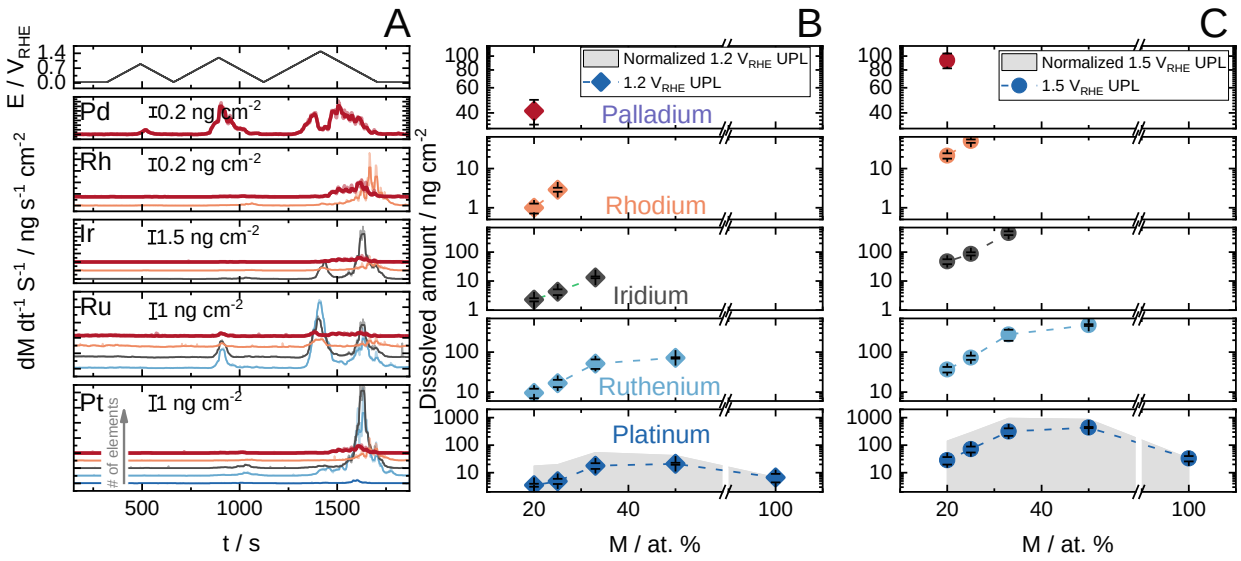

Fig. S15. Dissolution profiles recorded for the *carbon-supported metal alloy nanoparticles* in alkaline media and the calculated dissolved amounts as the function of the molar fraction of each metal in the alloy samples. (A) The protocol started with a five min hold at 0.05 V_{RHE}, which was followed by an additional potentiostatic hold for ten minutes at 1.2 V_{RHE}. The measurement was finished with a five min potentiostatic hold at 0.05 V_{RHE}. The electrolyte was 0.05 M KOH) in the case of both protocols and it was saturated with Ar during the measurements. In each panel, the dissolution profile at the bottom corresponds to either the pristine metal (only for Pt) or to the alloy comprised of the lowest number of elements. The topmost dissolution profile for each element corresponds to the PtRuIrRhPd HEA sample (red, in bold). Dissolution profiles were smoothed using an FFT filter (points of window = 5-8). The original dataset is presented behind the smoothed profile with 50% transparency. (B) and (C) Dissolved amounts as the function of the molar fraction of the given element in the alloy samples. Dissolved amounts were calculated by integrating the dissolution profiles presented in Figure 15A (0.05 M KOH electrolyte). Full diamonds – dissolved amount of the given metal during the second cycle *UPL* = 1.2 V_{RHE}, full circles – dissolved amount of the given metal during the second cycle *UPL* = 1.5 V_{RHE}. The grey shaded area represents the normalized dissolved amounts determined by dividing the calculated dissolved amounts with the molar fraction of the given element in the given alloy. Error bars were calculated from at least two separate measurements; each was performed on a fresh catalyst spot. Related to Figure 5.

References

1. Cherevko, S., Zeradjanin, A.R., Keeley, G.P., and Mayrhofer, K.J.J. (2014). A Comparative Study on Gold and Platinum Dissolution in Acidic and Alkaline Media. Journal of The Electrochemical Society *161*, H822-H830. 10.1149/2.0881412jes.
2. Cherevko, S. (2018). Electrochemical Dissolution of Noble metals. Elsevier Inc., 69-75.
3. Cherevko, S., Keeley, G.P., Geiger, S., Zeradjanin, A.R., Hodnik, N., Kulyk, N., and Mayrhofer, K.J. (2015). Dissolution of Platinum in the Operational Range of Fuel Cells. ChemElectroChem *2*, 1471-1478. 10.1002/celc.201500098.
4. Speck, F.D., Zagalskaya, A., Alexandrov, V., and Cherevko, S. (2021). Periodicity in the Electrochemical Dissolution of Transition Metals. Angew Chem Int Ed Engl *60*, 13343-13349. 10.1002/anie.202100337.
5. Schalenbach, M., Kasian, O., Ledendecker, M., Speck, F.D., Mingers, A.M., Mayrhofer, K.J.J., and Cherevko, S. (2017). The Electrochemical Dissolution of Noble Metals in Alkaline Media. Electrocatalysis *9*, 153-161. 10.1007/s12678-017-0438-y.
6. Hodnik, N., Jovanovič, P., Pavlišič, A., Jozinović, B., Zorko, M., Bele, M., Šelih, V.S., Šala, M., Hočevar, S., and Gaberšček, M. (2015). New Insights into Corrosion of Ruthenium and Ruthenium Oxide Nanoparticles in Acidic Media. The Journal of Physical Chemistry C *119*, 10140-10147. 10.1021/acs.jpcc.5b01832.
7. Pourbaix, M. (1974). Atlas of Electrochemical Equilibria in Aqueous Solutions.
8. Cherevko, S. (2017). Electrochemical dissolution of noble metals native oxides. Journal of Electroanalytical Chemistry *787*, 11-13. 10.1016/j.jelechem.2017.01.029.
9. Kormányos, A., Savan, A., Ludwig, A., Speck, F.D., Mayrhofer, K.J.J., and Cherevko, S. (2021). Electrocatalytic oxidation of 2-propanol on PtxIr100-x bifunctional electrocatalysts – A thin-film materials library study. Journal of Catalysis *396*, 387-394. 10.1016/j.jcat.2021.02.021.
10. Cherevko, S., Geiger, S., Kasian, O., Mingers, A., and Mayrhofer, K.J.J. (2016). Oxygen evolution activity and stability of iridium in acidic media. Part 1. – Metallic iridium. Journal of Electroanalytical Chemistry *773*, 69-78. 10.1016/j.jelechem.2016.04.033.
11. Kasian, O., Grote, J.P., Geiger, S., Cherevko, S., and Mayrhofer, K.J.J. (2018). The Common Intermediates of Oxygen Evolution and Dissolution Reactions during Water Electrolysis on Iridium. Angew Chem Int Ed Engl *57*, 2488-2491. 10.1002/anie.201709652.
12. Nørskov, J.K., Rossmeisl, J., Logadottir, A., Lindqvist, L., Kitchin, J.R., Bligaard, T., and Jónsson, H. (2004). Origin of the Overpotential for Oxygen Reduction at a Fuel-Cell Cathode. The Journal of Physical Chemistry B *108*, 17886-17892. 10.1021/jp047349j.
13. Shao, M., Odell, J., Humbert, M., Yu, T., and Xia, Y. (2013). Electrocatalysis on Shape-Controlled Palladium Nanocrystals: Oxygen Reduction Reaction and Formic Acid Oxidation. The Journal of Physical Chemistry C *117*, 4172-4180. 10.1021/jp312859x.
14. Zhang, J., Chen, M., Li, H., Li, Y., Ye, J., Cao, Z., Fang, M., Kuang, Q., Zheng, J., and Xie, Z. (2018). Stable palladium hydride as a superior anode electrocatalyst for direct formic acid fuel cells. Nano Energy *44*, 127-134. 10.1016/j.nanoen.2017.11.075.
15. Pizzutilo, E., Freakley, S.J., Geiger, S., Baldizzone, C., Mingers, A., Hutchings, G.J., Mayrhofer, K.J.J., and Cherevko, S. (2017). Addressing stability challenges of using bimetallic electrocatalysts: the case of gold–palladium nanoalloys. Catalysis Science & Technology *7*, 1848-1856. 10.1039/c7cy00291b.